

P. Mahanta et al. (eds.), *Advances in Thermofluids and Renewable Energy, Lecture Notes in Mechanical Engineering*, Springer Nature Singapore Pte Ltd.

Accepted August 13th 2021

PERTURBATION AND MAPLE QUADRATURE COMPUTATION OF THERMO-SOLUTAL DISSIPATIVE REACTIVE CONVECTIVE FLOW IN A GEOTHERMAL DUCT WITH ROBIN BOUNDARY CONDITIONS:

J.C. Umavathi

Visiting Professor, Dipartimento di Ingegneria dell'Università degli Studi della Campania "Luigi Vanvitelli", Via Roma 29, Italy.

O. Anwar Bég

Professor of Engineering Science, Department of Mechanical Engineering, SEE, University of Salford, Manchester, M5 4WT, UK.

B. Vasu*

Department of Mathematics, Motilal Nehru National Institute of Technology Allahabad, Prayagraj, Uttar Pradesh, India.

R. S. R. Gorla

Professor of Aerospace Engineering, US Air Force Institute of Technology, Dayton, Ohio, USA.

*** Corresponding Author**

ABSTRACT

Buoyancy-driven reactive flows feature extensively in geophysics, materials processing and energy systems. In respect to the latter, geothermal energy holds great promise in India and other Asian geographical locations and offers immense resources in the 21st century. Motivated by such applications, in the current study a mathematical model is developed for thermo-solutal convection flow in an open two-dimensional vertical channel containing a porous medium saturated with reactive Newtonian fluid is studied. Robin boundary conditions are prescribed and a first order homogenous chemical reaction is considered. The Darcy-Forchheimer model is used to simulate both first and second order porous medium drag effects. The reference temperatures are taken as symmetric or asymmetric. Viscous heating is also included in the model. The conservation equations are written in dimensionless form taking into account the effects of viscous dissipation. For the case of small Brinkman number (i.e. viscous heating parameter) and neglecting the Forchheimer quadratic drag effect, perturbation solution of the simpler Darcian boundary value problem is developed. For the general non-Darcy-case, a numerical solution is presented with the Runge-Kutta quadrature and a shooting method. Good correlation between analytical and numerical solutions is demonstrated. The influence of thermal and solute Grashof numbers, Biot numbers, Brinkman number, first order chemical reaction parameter, porous medium parameter and Forchheimer (inertial drag) parameter on velocity, temperature and concentration (species) distributions is visualized graphically. Nusselt number and skin friction at the walls are computed for selected parameters relevant to real geothermics. Increasing porous media parameter (decreasing medium permeability) reduces temperatures for both equal and unequal Biot numbers. Increasing thermal Grashof number accelerates the flow and elevates temperatures for both equal and unequal Biot numbers. With higher values of solutal Grashof number velocity and temperature near the cold plate (wall) are reduced whereas the converse behaviour is induced at the hot wall. Increasing chemical reaction parameter elevates the species concentration in the left half space of the channel whereas it suppresses concentration in the right half space and in both scenarios a parabolic distribution is observed. In the absence of chemical reaction, a linear growth in concentration is computed from the left plate to the right plate. With increasing porous medium parameter and Forchheimer inertial parameter the flow is strongly decelerated across the channel span whereas there is a much weaker reduction in temperatures. Skin friction is consistently lowered at both plates with increasing thermal Grashof number for equal Biot numbers. However, with unequal Biot numbers, skin friction at the left plate is increased whereas it is still reduced at the right plate. With increasing solutal Grashof number, skin friction is always reduced at both plates for both equal and unequal Biot numbers. There is also a consistent decrease in Nusselt numbers at both plates with increasing solutal Grashof number.

KEYWORDS: *Geothermal reactive systems; Non-Darcy porous medium, Robin boundary conditions, perturbation method; thermosolutal buoyancy; convection; chemical reaction; Runge-Kutta method; Nusselt number.*

LIST OF SYMBOLS

A	constant
Bi_1, Bi_2	Biot numbers at the left and right channel walls
Br	Brinkman number
c_p	specific heat at constant pressure
C_F	Forchheimer drag term
D	Hydraulic diameter, $2L$
g	acceleration due to gravity
I	inertial parameter
λ_1	thermal Grashof number
λ_2	solatal (species) Grashof number
h_1, h_2	external heat transfer coefficients
K	thermal conductivity of the fluid
K_m	dimensional chemical reaction parameter
L	channel width
Nu_1, Nu_2	Nusselt numbers at the left and right channel walls
P	Pressure
$P = p + \rho_0 g X$	difference between the pressure and the hydrostatic pressure
Re	Reynolds number
R_r	temperature difference ratio
S	dimensionless parameter
T	temperature
T_1, T_2	reference temperatures of the external fluid
T_0	reference temperature
u	dimensionless velocity in the X - direction
U	velocity component in the X - direction
U_0	reference velocity
X	stream wise coordinate
y	dimensionless transverse coordinate
Y	transverse coordinate

Greek symbols

α	chemical reaction parameter
β_T	thermal expansion coefficient
β_C	concentration expansion coefficient
ΔT	reference temperature difference
ε	dimensionless parameter
θ	dimensionless temperature
ϕ	dimensionless concentration
ρ	density of the fluid
ρ_0	value of the mass density when $T = T_0$

μ	dynamic viscosity
ν	kinematic viscosity
σ	porous media permeability parameter

1. INTRODUCTION

Thermosolutal buoyancy-driven flows are mobilized by variations in density variation induced by species concentration and temperature. Such flows which feature coupled heat and mass transfer often arise in porous media. Applications of these “double-diffusive” flows include geothermal energy systems (**Fig. 1a**), contamination fate in soils, petrochemical reservoir dynamics and chromatography. Double-diffusive natural convection in confined porous media is also of relevance in fuel combustion (e.g. forest fires), thermal insulation, materials processing, room ventilation, packed-bed chemical reactors etc.

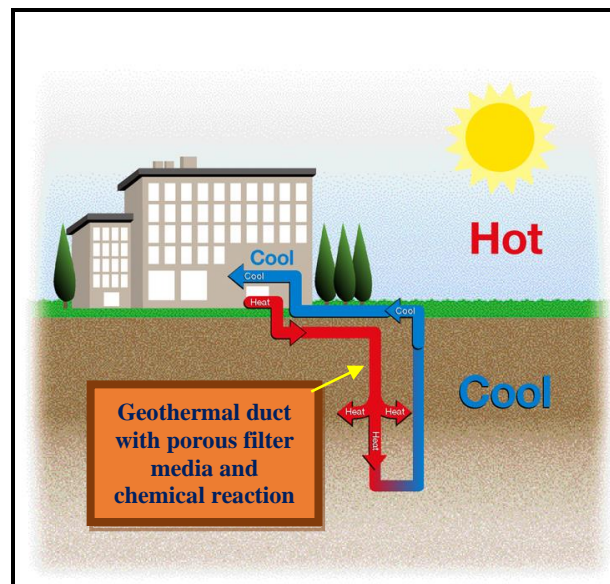


Fig 1a: Schematic of a geothermal duct with porous media and reactive flow

Thermosolutal transport in porous media has been reviewed extensively by Kaviany [1], Nield and Bejan [2] and Ingham and Pop [3], who have provided an excellent range of modelling approaches and identified many new emerging areas of application of both internal flows (cavities, channels, heat pipes) and external boundary layer flows (polymer fabrication, spray deposition, filtration etc). Many further geological applications of heat and mass transfer in permeable media have been reviewed by Phillips [4]. Interesting studies of double-diffusive convection in porous media include Gupta *et al.* [5] (on transient micropolar flow in isotropic permeable materials), Mamou *et al.* [6] (on buoyancy-driven heat and mass transfer in a saturated vertical porous media cavity) and Narayana and Murthy [7] (on cross-diffusion in thermo-solutal boundary layer flow in homogenous porous media).

In porous media hydrodynamics, the traditional approach is to use the Darcy law which provides the linear relationship between the pressure drop across the porous medium and the Darcian velocity. This model is however only valid for low Reynolds numbers i.e. viscous dominated “creeping” flows. It has been deployed extensively in recent years in a multiplicity of applications. Relevant studies include Prasad and Kulacki [8], Vasseur *et al.* [9], and Umavathi *et al.* [10]-[13]. The Darcy model utilized in these investigations has also considered the porous matrix to be isotropic and homogenous. At higher velocities (which may arise in high-permeability geological formations for example), inertial effects dominate the viscous effect. The the pressure drop becomes a quadratic function of the flow rate and a

non-Darcy model is required. Two popular methodologies for non-Darcy models have emerged i.e. *Brinkman-extended Darcy models* [19] and *Forchheimer-extended Darcy models* [20]. These are accommodated well in viscous fluid dynamic models and respectively simulate the viscous stresses adjacent to the bounding walls (“vorticity diffusion”) and channeling effects, and the *non-linear drag* effect generated by the solid matrix fibers at higher velocities. Since the inclusion of a Forchheimer quadratic term renders the momentum equation nonlinear, generally numerical methods are required for deriving solutions. Many researchers have implemented the Darcy-Forchheimer model in recent years in both thermal convection and thermo-solutal convection simulations. Bég *et al.* [21] conducted network electro-thermal computational simulations of Sakiadis flow in a thermally-stratified Darcy-Forchheimer medium with the PSPICE code. Chen [22] used a cubic spline collocation method to investigate the influence of Forchheimer quadratic drag on thermosolutal convection boundary layer flow from a vertical wavy surface in a non-Darcy fluid-saturated porous medium. Jena *et al.* [23] employed a finite control volume integration technique to study the combined heat and mass transfer in a fluid-saturated porous medium composite enclosure with a Darcy-Brinkman-Forchheimer model. Bég *et al.* [24] applied the Differential transform method (DTM) to compute buoyancy effects in dusty physiological thermo-convection in a Darcy-Forchheimer vertical porous medium channel. These studies all confirmed the significant modification in transport characteristics both in the bulk flow and at the walls induced with Forchheimer quadratic drag. A rigorous theoretical validation of the Darcy-Forchheimer model has been presented by Chen *et al.* [25] via homogenization theory and Whittaker [26] with asymptotic methods. Experimental corroboration of this model has also been presented by Sener *et al.* [27].

In many geological and engineering systems featuring double-diffusive convection, chemical reaction effects arise. Geochemical flows include precipitation reaction (e.g. acidic brine and a calcium feldspar), mineralogical dissolution, carbon dioxide injection [28], brine chemo-geothermics in domestic heating systems [29] and pollutant leaching [30]. Further examples in industrial technologies include polymer radical manipulation, catalytic conversion, exothermic chemical reactions in porous media reactors [31], time-dependent corrosion of metallic components [32] and materials synthesis [33]. Mathematical models of reactive flows usually feature either homogeneous or heterogeneous chemical reactions. Homogeneous reactions occur in one phase only whereas heterogeneous reactions occur in two or more phases. Either type may be destructive or constructive. In more complex systems, autocatalytic reactions may also arise in which the reaction product acts as the catalyst for the chemical reaction. Considerable activity in modelling laminar reactive double-diffusive convection flows has emerged in recent years. Anjali Devi and Kandasamy [34] investigated natural convection boundary layer flow with higher order chemical reaction. They showed that with stronger chemical reaction and decreasing Schmidt number there is an acceleration in the flow and depletion in concentration gradient at the wall. Reactive flows in porous media have also been explored extensively. Postelnicu [35] used a finite difference technique to study the influence of order of homogenous chemical reaction, chemical reaction rate parameter and sustentation parameter on thermosolutal reactive flow in a Darcy medium with cross-diffusion effects. Rashad and El-Kabeir [36] deployed a Runge-Kutta integration scheme with shooting method to compute the chemical reaction effects in unsteady non-isothermal, non-isolutal flow from a stretching sheet embedded in a Darcian porous medium. Kandasamy *et al.* [37] considered variable viscosity and thermophoresis effects on mixed double-diffusive convection in Falkner-Skan flow from a wedge in a non-Darcy porous medium with first order homogeneous chemical reaction. They noted that species concentration is suppressed with increasing reaction parameter and that opposing buoyancy reduces wall mass transfer rates. Zueco *et al.* [38] studied the effects of Forchheimer inertial drag and permeability on thermosolutal convection from a cylindrical body with homogenous chemical reaction. Nguyen *et al.* [39] used Fourier spectral element and hybrid Adams-Bashforth and backward Euler numerical schemes to investigate the thermal convection in a fluid-saturated non-Darcy

anisotropic porous medium generated by a surface nth order irreversible reaction. They showed that Forchheimer drag and chemical reaction modify the momentum, heat and species diffusion characteristics substantially.

Convective heat exchange at a bounding surface is also an important consideration in thermo-solutal convection flows. It arises in transpiration cooling processes, cooling or heating of geological strata, material drying, heat exchangers, geothermal bore wells etc. Very few studies have incorporated the *Robin boundary condition* i.e. mixed boundary condition. Also known as the boundary condition of the third kind, inclusion of this type of boundary condition has been shown to produce results which deviate non-trivially from those computed with classical isothermal or isosolutal boundary conditions. Zanchini [40] was among the first researchers to analyze in detail with a perturbation method, the fully developed mixed convection in a parallel-plate vertical channel in which the walls exchange heat with an external fluid. He applied Robin boundary conditions (also known as boundary conditions of the third kind) and considered both conditions of equal and of different reference temperatures of the external fluid and furthermore included viscous heating effects. Building on Zanchini's work, Umavathi *et al.* [41] considered the supplementary effects of heat generation and absorption. Umavathi *et al.* [42] further extended the Zanchini model to consider non-Darcy effects.

In the present investigation, a mathematical model is developed to study the collective effects of first order homogeneous chemical reaction on double-diffusive convection in a viscous fluid flowing in a vertical duct containing an isotropic, homogenous porous medium. The Brinkman-Forchheimer extended Darcy model is employed and Robin boundary conditions are imposed. This work therefore further generalizes the study in [42] to consider chemical reaction and viscous heating effects. Viscous heating is known to arise in a number of geological applications including mantle convection [43] and enhanced oil recovery [44]. Both perturbation and numerical solutions are presented, the former for the case of small Brinkman number (dissipation parameter) in the absence of Forchheimer inertial drag. Extensive visualization of the influence of non-Darcy, buoyancy, reaction, dissipation and boundary conditions on momentum, species and heat transfer characteristics are provided.

2. MATHEMATICAL GEOTHERMAL REACTIVE DUCT FLOW MODEL

Steady-state, incompressible, fully developed flow driven by buoyancy due to temperature and concentration gradients in a vertical channel containing a saturated non-Darcy porous medium is considered. Viscous dissipation and first order homogenous chemical reaction of the solute are assumed. An (X,Y) coordinate system is employed and the origin is located at the mid-plane of the channel. The distance between the plates is L as shown in the geothermal duct model i.e. **Figure 1b**. The fluid properties are assumed to be constant except for density variations in the buoyancy force terms. Thermal dispersion, cross-diffusion and stratification effects are neglected. In addition, the concentration of the solute constituent in the solution that saturates the porous medium at the left wall is C_1 and at the right wall is C_2 in such way that $C_2 \geq C_1$. The velocity is taken as zero on the walls of the duct. The duct walls are infinite in the X -direction. Therefore the flow become one-dimensional along the X -axis, and hence velocity is a function of Y only. The governing equations for momentum, energy and species conservation with the Darcy-Forchheimer model after adopting the Boussinesq approximations may be shown to take the form:

$$\rho_0 g \beta_T (T - T_0) + \rho_0 g \beta_C (C - C_0) - \frac{\partial p}{\partial X} + \mu \frac{d^2 U}{dY^2} - \frac{\mu}{\kappa} U - \frac{\rho C_F}{\sqrt{\kappa}} U^2 = 0 \quad (1)$$

$$K \frac{d^2 T}{dY^2} + \mu \left(\frac{dU}{dY} \right)^2 + \frac{\mu}{\kappa} U^2 = 0 \quad (2)$$

$$D_m \frac{d^2 C}{dY^2} - K_m C = 0 \quad (3)$$

The thickness of the channel walls is neglected and the walls are assumed to exchange convective heat with the external fluid. The convective heat co-efficient is taken as h_1 at the left wall and h_2 at the right wall of the duct (channel). The reference temperature is T_1 at $Y = -L/2$ and T_2 at $Y = L/2$ such that $T_2 \geq T_1$. The pressure gradient is treated as constant $\left(\frac{\partial P}{\partial X} = A\right)$. With these assumptions the conditions on the boundary for the velocity, temperature and concentration now can be written as:

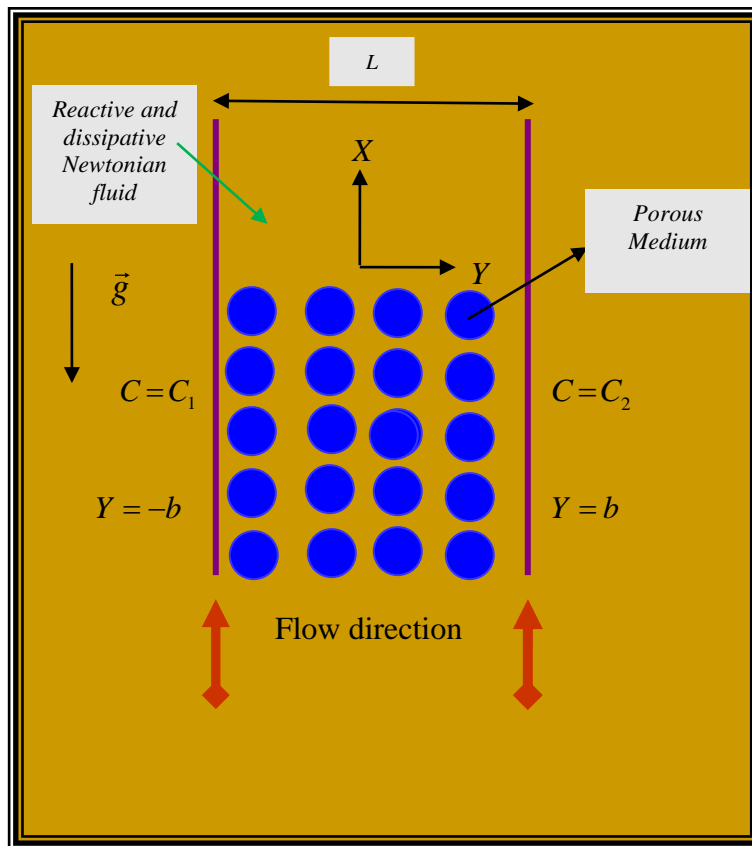


Figure 1b. Schematic diagram of thermosolutal reactive convection in vertical porous medium geothermal duct

$$U\left(-\frac{L}{2}\right) = U\left(\frac{L}{2}\right) = 0 \quad (5)$$

$$-K\left(\frac{dT}{dY}\right)_{Y=-\frac{L}{2}} = h_1\left[T_1 - T\left(X, -\frac{L}{2}\right)\right], \quad -K\left(\frac{dT}{dY}\right)_{Y=\frac{L}{2}} = h_2\left[T\left(X, \frac{L}{2}\right) - T_2\right] \quad (4)$$

$$C\left(-\frac{L}{2}\right) = C_1, \quad C\left(\frac{L}{2}\right) = C_2 \quad (6)$$

It is pertinent to invoke the following dimensionless parameters:

$$\begin{aligned}
u &= \frac{U}{U_0}; \quad \theta = \frac{T-T_0}{\Delta T}; \quad y = \frac{Y}{D}; \quad GR_T = \frac{g\beta_T\Delta TD^3}{\nu^2}; \quad GR_C = \frac{g\beta_C\Delta TD^3}{\nu^2}; \quad Re = \frac{U_0 D}{\nu} \\
Br &= \frac{\mu U_0^2}{K\Delta T}; \quad R_T = \frac{T-T_0}{\Delta T}; \quad Bi_1 = \frac{h_1 D}{K}; \quad Bi_2 = \frac{h_2 D}{K}; \quad \sigma = \frac{D}{\sqrt{\kappa}}; \quad U_0 = \frac{-AD^2}{48\mu} \\
\alpha &= \frac{K_m D^2}{D_m}; \quad S = \frac{Bi_1 Bi_2}{Bi_1 Bi_2 + 2Bi_1 + 2Bi_2}; \quad \phi = \frac{C-C_0}{\Delta C}; \quad I = \frac{\rho C_F D^2 U_0}{\mu \sqrt{\kappa}}; \quad D = 2L \\
T_0 &= \frac{T_1 + T_2}{2} + S \left(\frac{1}{Bi_1} - \frac{1}{Bi_2} \right) (T_2 - T_1); \quad \lambda_1 = \frac{GR_T}{Re}; \quad \lambda_2 = \frac{GR_C}{Re}; \quad \Delta T = T_2 - T_1; \quad \Delta C = C_2 - C_1; \\
C_0 &= \frac{C_1 + C_2}{2}
\end{aligned} \tag{7}$$

Implementing Eqn. (7) in Eqns. (1)–(6) yields the following system of coupled ordinary differential equations:

$$\frac{d^2 u}{dy^2} + \lambda_1 \theta + \lambda_2 \phi + 48 - \sigma^2 u - I u^2 = 0 \tag{8}$$

$$\frac{d^2 \theta}{dy^2} + Br \left(\frac{du}{dy} \right)^2 + \sigma^2 Br u^2 = 0 \tag{9}$$

$$\frac{d^2 \phi}{dy^2} - \alpha^2 \phi = 0 \tag{10}$$

The associated boundary conditions are:

$$u \left(-\frac{1}{4} \right) = u \left(\frac{1}{4} \right) = 0 \tag{11}$$

$$\left(\frac{d\theta}{dy} \right)_{y=-\frac{1}{4}} = Bi_1 \left(\theta \left(-\frac{1}{4} \right) + \frac{R_T S}{2} \left(1 + \frac{4}{Bi_1} \right) \right), \quad \left(\frac{d\theta}{dy} \right)_{y=\frac{1}{4}} = Bi_2 \left(-\theta \left(\frac{1}{4} \right) + \frac{R_T S}{2} \left(1 + \frac{4}{Bi_2} \right) \right) \tag{12}$$

$$\phi \left(-\frac{1}{4} \right) = -0.5, \quad \phi \left(\frac{1}{4} \right) = 0.5 \tag{13}$$

Here all parameters are defined in the notation.

3. PERTURBATION SOLUTION METHOD

The closed form solution of the linear species diffusion Eqn. (10) is readily obtained:

$$\phi = \frac{\text{Sinh}(\alpha y)}{2 \text{Sinh}(\alpha / 4)} \tag{14}$$

However, the problem represented by Eqns. (8) and (9) i.e. the transformed momentum and energy equations, is nonlinear and has no closed form solutions. Therefore, approximate solutions are determined using a regular perturbation method (RPM). These solutions are valid (in the absence of inertial effects) only for small values of the dissipation parameter i.e. Brinkman number (Br) which is taken as the perturbation parameter. The solutions of Eqns. (8) and (9) can be expressed as:

$$u = u_0 + Br u_1 + Br^2 u_2 + Br^3 u_3 + \dots \quad (15)$$

$$\theta = \theta_0 + Br \theta_1 + Br^2 \theta_2 + Br^3 \theta_3 + \dots \quad (16)$$

Substituting the above expansions (15) and (16) in Eqns. (8), (9), (11) and (12) and equating the like powers of Br one obtains the following equations:

Zeroth order equations ($Br = 0$)

$$\frac{d^2 u_0}{dy^2} - \sigma^2 u_0 + \lambda_1 \theta_0 + \lambda_2 \phi + 48 = 0 \quad (17)$$

$$\frac{d^2 \theta_0}{dy^2} = 0 \quad (18)$$

$$u_0 \left(-\frac{1}{4} \right) = u_0 \left(\frac{1}{4} \right) = 0 \quad (19)$$

$$\left(\frac{d\theta_0}{dy} \right)_{y=-\frac{1}{4}} = Bi_1 \left(\theta_0 \left(-\frac{1}{4} \right) + \frac{R_T S}{2} \left(1 + \frac{4}{Bi_1} \right) \right), \quad \left(\frac{d\theta_0}{dy} \right)_{y=-\frac{1}{4}} = Bi_2 \left(-\theta_0 \left(\frac{1}{4} \right) + \frac{R_T S}{2} \left(1 + \frac{4}{Bi_2} \right) \right) \quad (20)$$

The closed form solutions of Eqns. (17) and (18) using boundary conditions (19) and (20) emerge as:

$$\theta_0 = c_3 + c_4 y \quad (21)$$

$$u_0 = c_5 \text{Cosh}(\sigma y) + c_6 \text{Sinh}(\sigma y) + d_1 \text{Sinh}(\alpha y) + d_2 y + d_3 \quad (22)$$

First order equations ($Br = 1$)

$$\frac{d^2 u_1}{dy^2} - \sigma^2 u_1 + \lambda_1 \theta_1 = 0 \quad (23)$$

$$\frac{d^2 \theta_1}{dy^2} + \left(\frac{du_0}{dy} \right)^2 + \sigma^2 u_0^2 = 0 \quad (24)$$

$$u_1 \left(-\frac{1}{4} \right) = u_1 \left(\frac{1}{4} \right) = 0 \quad (25)$$

$$\left(\frac{d\theta_1}{dy} \right)_{y=-\frac{1}{4}} = Bi_1 (\theta_1)_{y=-\frac{1}{4}}, \quad \left(\frac{d\theta_1}{dy} \right)_{y=\frac{1}{4}} = -Bi_2 (\theta_1)_{y=\frac{1}{4}} \quad (26)$$

The closed form solutions of Eqns. (23) and (24) using boundary conditions (25) and (26) are:

$$\begin{aligned} \theta_1 = & g_1 \text{Cosh}(2\sigma y) + g_2 \text{Sinh}(2\sigma y) + g_3 \text{Cosh}(2\alpha y) + g_4 \text{Cosh}((\sigma + \alpha)y) + \\ & g_5 \text{Cosh}((\sigma - \alpha)y) + g_6 y \text{Sinh}(\alpha y) + g_7 \text{Cosh}(\alpha y) + g_8 \text{Sinh}(\sigma y) + \\ & g_9 \text{Cosh}(\sigma y) + g_{10} y^4 + g_{11} y^3 + g_{12} y^2 + c_7 y + c_8 \end{aligned} \quad (27)$$

$$\begin{aligned}
u_1 = & c_9 \text{Cosh}(\sigma y) + c_{10} \text{Sinh}(\sigma y) + f_1 \text{Cosh}(2\sigma y) + f_2 \text{Sinh}(2\sigma y) + f_3 \text{Cosh}(2\alpha y) + \\
& f_4 \text{Cosh}((\sigma + \alpha) y) + f_5 \text{Cosh}((\sigma - \alpha) y) + f_6 y \text{Sinh}(\alpha y) + f_7 y \text{Cosh}(\sigma y) + \\
& f_8 y \text{Sinh}(\sigma y) + f_9 \text{Cosh}(\alpha y) + f_{10} y^4 + f_{11} y^3 + f_{12} y^2 + f_{13} y + f_{14}
\end{aligned} \quad (28)$$

4. MAPLE QUADRATURE NUMERICAL SOLUTIONS

The approximate analytical solutions obtained are valid only for small values of Brinkman number and in the absence of inertia forces. To relax this condition on Brinkman number and to evaluate the effects of porous medium inertial drag (Forchheimer second order impedance) on the flow, the momentum and energy Eqns. (8) and (9) are solved numerically using an efficient Runge-Kutta procedure with an appropriate shooting method. This may be executed in any number of symbolic software including Maple, Mathematica and Matlab. Details of this technique are given in [45]-[47]. **MAPLE** has been used in the geothermal duct simulation. The stepping formulae although designed for nonlinear problems, are even more efficient for any order of linear differential equation and are summarized below:

$$k_0 = f(x_i, y_i), \quad (29)$$

$$k_1 = f\left(x_i + \frac{1}{4}h, y_i + \frac{1}{4}hk_0\right), \quad (30)$$

$$k_2 = f\left(x_i + \frac{3}{8}h, y_i + \left(\frac{3}{32}k_0 + \frac{9}{32}k_1\right)h\right), \quad (31)$$

$$k_3 = f\left(x_i + \frac{12}{13}h, y_i + \left(\frac{1932}{2197}k_0 - \frac{7200}{2197}k_1 + \frac{7296}{2197}k_2\right)h\right), \quad (32)$$

$$k_4 = f\left(x_i + h, y_i + \left(\frac{439}{216}k_0 - 8k_1 + \frac{3860}{513}k_2 - \frac{845}{4104}k_3\right)h\right), \quad (33)$$

$$k_5 = f\left(x_i + \frac{1}{2}h, y_i + \left(-\frac{8}{27}k_0 + 2k_1 - \frac{3544}{2565}k_2 + \frac{1859}{4101}k_3 - \frac{11}{40}k_4\right)h\right), \quad (34)$$

$$y_{i+1} = y_i + \left(\frac{25}{216}k_0 + \frac{1408}{2565}k_2 + \frac{2197}{4101}k_3 - \frac{1}{5}k_4\right)h, \quad (35)$$

$$z_{i+1} = z_i + \left(\frac{16}{135}k_0 + \frac{6656}{12825}k_2 + \frac{28561}{56430}k_3 - \frac{9}{50}k_4 + \frac{2}{55}k_5\right)h. \quad (36)$$

Here y denotes fourth order Runge-Kutta phase and z is the fifth order Runge-Kutta phase. An estimate of the error is achieved by subtracting the two values obtained. If the error exceeds a specified threshold, the results can be re-calculated using a smaller step size. The approach to estimating the new step size is shown below:

$$h_{new} = h_{old} \left(\frac{\varepsilon h_{old}}{2|z_{i+1} - y_{i+1}|} \right)^{1/4}. \quad (37)$$

The solutions obtained by the numerical scheme (RKM) are used to validate the perturbation solutions (RPM), for small values of Brinkman number. Excellent correlation is obtained as described in due course (Tables 3 and 4).

5 ENERGY DESIGN QUANTITIES - SKIN FRICTION AND NUSSELT NUMBER

The dimensionless skin friction (surface shear stress i.e. velocity gradient) and Nusselt number (surface heat transfer rate i.e. temperature gradient) are given by:

$$\tau_1 = \left(\frac{du}{dy} \right)_{y=-\frac{1}{4}}, \quad \tau_2 = \left(\frac{du}{dy} \right)_{y=\frac{1}{4}} \quad (38)$$

$$Nu_1 = \left(\frac{d\theta}{dy} \right)_{y=-\frac{1}{4}}, \quad Nu_2 = \left(\frac{d\theta}{dy} \right)_{y=\frac{1}{4}} \quad (39)$$

6. RESULTS AND DISCUSSION

Figures 2-23 display the profiles for the velocity, temperature and solute concentration obtained with the numerical method (RKM). These results illustrate the effects of Brinkman number Br , thermal Grashof number λ_1 , solutal (concentration) Grashof number λ_2 , chemical reaction parameter α , Forchheimer inertial parameter I for different values of porous parameter σ , Biot numbers and temperature difference ratio R_T . Eqns. (8) to (10) along with boundary conditions (11) to (13) are solved analytically using the regular perturbation method (RPM) which is valid when Brinkman number is less than one and numerically with the Runge-Kutta and shooting method (RKM) which can be employed for any values of Brinkman number.

The effects of thermal Grashof number λ_1 and porous medium parameter σ on the velocity and temperature characteristics are shown in **Figs. 2 to 4**. In the absence of viscous dissipation ($Br = 0$), there is a flow reversal near the cold wall for strong thermal buoyancy cases with values of $\lambda_1 = 500, 1000$. Figure 2 also indicates that increasing porous medium parameter σ decelerates the flow for all values of thermal Grashof number, λ_1 . $\sigma = \frac{D}{\sqrt{\kappa}}$ and evidently this parameter is inversely

proportional to the medium permeability, κ . It arises in the Darcian linear impedance term in the normalized momentum eqn. (8) i.e. $-\sigma^2 u$. Clearly as σ increases the medium permeability is reduced and this increases the resistance of porous medium fibers (fabric) to the flow. Velocity is therefore depleted. The temperature profiles as seen Figs. 3 and 4 are drawn for different values of Brinkman number Br and porous parameter σ in the absence of thermal Grashof number λ_1 for equal and unequal Biot numbers. In the absence of viscous dissipation, the temperature profile is linear as the heat transfer contribution is dominated by thermal conduction. The effect of viscous dissipation ($Br \neq 0$) is to increase the temperature field for equal and unequal Biot numbers. This is due to the conversion of kinetic energy into heat via viscous heating which increases temperatures in the regime. However, the nature of profiles is markedly different for equal and unequal Biot numbers. There is a convective heat transfer domination over conduction heat transfer in the boundary layer region adjacent to the walls. Figures 3 and 4 also imply that the effect of increasing permeability parameter σ is to reduce the temperature magnitudes for both equal (symmetric case) and unequal (asymmetric case) Biot numbers. Decreasing permeability offers less fluid volume for thermal convection and greater solid fibers for thermal conduction. This cools the regime. The results obtained in Figs. 2 to 4 in the

absence of porous medium parameter, inertial parameter and concentration Grashof number are similar to those obtained by Zanchini [40].

The impact of thermal Grashof number on velocity and temperature evolution in the regime is illustrated in Figs. 5 to 8 for various values of Brinkman number Br and porous medium parameter σ . The effect of viscous dissipation (simulated in the nonlinear term, $\sigma^2 Bru^2$ in the energy eqn. (9)) is to enhance the flow for all values of porous medium parameter σ and Biot numbers (Bi_1 and Bi_2). The large values of σ as noted earlier, decrease medium permeability and therefore inhibit thermal convection. The frictional drag resistance and inertial quadratic drag significantly retard the flow for both equal and unequal Biot numbers. Temperatures are significantly elevated with greater Brinkman number and higher magnitudes are obtained for the asymmetric Biot number case (fig. 8) compared with the symmetric Biot number case (fig. 6). Evidently therefore the inclusion of Robin boundary conditions produces substantially different magnitudes compared with conventional boundary conditions.

The effect of thermal Grashof number λ_1 and porous parameter σ on the velocity and temperature fields are displayed in Figs. 9 to 12 for equal and unequal Biot numbers. The effect of thermal Grashof number λ_1 is to enhance the velocity and temperature fields for both equal and unequal Biot numbers. This is due to the fact that with higher values of thermal Grashof number there is an enhancement in thermal buoyancy force in the body force term, $+\lambda_1\theta$ in Eqn. (8) which serves to accelerate the flow, as noted in many studies including Gebhart *et al.* [48]. The effect of porous parameter σ is again to suppress the convection motion and reduce temperatures in the regime owing to the increased Darcian drag counteracting the flow for both equal and unequal Biot numbers.

The effect of concentration Grashof number λ_2 and porous parameter σ is shown in Figs. 13 and 14. As the concentration Grashof number λ_2 increases, the species buoyancy force modelled via the term $+\lambda_2\phi$ is increased. The velocity and temperature near the cold wall decreases, whereas it increases at the hot wall for different values of porous parameter σ . The effect of concentration Grashof number λ_2 on the velocity and temperature fields for unequal Biot numbers show a similar effect to that computed with equal Biot number (Figs. 13 and 14) and are therefore not included. The effect of chemical reaction parameter α on the concentration field is to increase the velocity field near the left wall and decrease it at the right wall as shown in Fig. 15. The impact of chemical reaction is therefore not consistent across the vertical channel span. The homogenous chemical reaction is both destructive (in the right half space) and constructive (in the left half space). Equation (10) implies that the concentration field is influenced only by the chemical reaction parameter α and remains invariant with the other parameters. In the absence of chemical reaction effect there is clearly a linear ascent in concentration from the left wall to the right wall. This is warped into an increasingly parabolic profile with stronger chemical reaction effect.

Figures 16 to 19 display the effect of Forchheimer inertial parameter I and porous medium parameter σ on the velocity and temperature distributions for equal and unequal Biot numbers. The effect of inertial parameter is to decelerate the flow for both equal and unequal Biot numbers. The impact of inertial parameter I is more prominent at smaller values of porous parameter σ as noted by Lai and Kulacki [48]. Clearly the neglect of Forchheimer second order drag leads to over-predictions in the velocity magnitudes. Temperatures are also strongly suppressed with increasing inertial parameter, I and the distributions for the both equal (symmetric) and unequal (asymmetric) Biot number cases are distinctly *monotonic* in nature at high permeability parameters (σ) whereas they are morphed into *parabolic profiles* at lower values of σ .

Figures 2 to 19 are drawn for asymmetric condition i.e. temperature difference ratio is non-zero ($R_T \neq 0$). To understand the flow nature for the symmetric condition ($R_T = 0$), the velocity and

temperature profiles are shown in Figs. 20 to 23 for equal and unequal Biot numbers and for different values of Brinkman number Br . The effect of Brinkman number for the *symmetric* condition is similar to that observed for the *asymmetric* condition (Figs. 5 to 8). That is to say that, Brinkman number *accelerates* the flow for equal and unequal Biot numbers whereas the porous medium parameter consistently *decelerates* the flow. The effect of Brinkman number for equal and unequal Biot numbers is again in good agreement with the nature of the results observed by Zanchni (1998) in the absence of porous medium and chemical reaction effects.

The values of skin friction and Nusselt numbers are shown in Tables 1 and 2 respectively for all the emerging thermophysical parameters for both equal and unequal Biot numbers. For equal Biot numbers, as the Brinkman number Br and chemical reaction parameter α are increased, skin friction increases at the left wall whereas it decreases at the right wall with greater values of thermal Grashof number λ_1 , solutal (concentration) Grashof number λ_2 , porous parameter σ and inertial parameter I . The skin friction at the right wall increases in magnitude with an elevation in values of thermal Grashof number, solutal Grashof number and Brinkman number whereas the converse behavior is observed with increasing the values of chemical reaction parameter, porous parameter and inertial parameter. A similar trend is computed for the asymmetric case of unequal Biot numbers.

The rate of heat transfer i.e. Nusselt number Nu_1 at the left wall increases with greater values of thermal Grashof number, Brinkman number and chemical reaction parameter whereas it decreases with concentration Grashof number, porous medium parameter and Forchheimer inertial parameter. The Nusselt number Nu_2 at the right wall however decreases with increasing the values of thermal Grashof number, concentration Grashof number and Brinkman number whereas it increases with chemical reaction parameter, porous medium parameter and Forchheimer inertial parameter. For unequal Biot numbers, Nu_1 increases with thermal Grashof number, Brinkman number and chemical reaction parameter, whereas it is reduced with increasing concentration Grashof number, porous medium parameter and Forchheimer inertial parameter. At the right wall, Nu_2 increases with thermal Grashof number, concentration Grashof number and Brinkman number whereas it decreases with chemical reaction parameter, porous medium parameter and Forchheimer inertial parameter.

The results illustrated in Figs 2-23 and Tables 1 and 2 are evaluated by solving the Eqs. (8) to (10) along with the boundary conditions (10) to (13) using the Runge-Kutta-Shooting method (RKM). To verify the solutions obtained by Runge-Kutta-Shooting method, a comparison is made with the analytical solutions obtained using regular perturbation method (RPM) in the absence of inertial effects. The comparisons are documented in Tables 3 and 4 for equal and unequal Biot numbers respectively. In the absence of Brinkman number, analytical and numerical solutions for the velocity, temperature and concentration fields *are the same for both cases* of equal and unequal Biot numbers. For equal Biot numbers and $Br = 0.01$, the analytical and numerical solutions agree to the three decimal places for the *velocity* field, one decimal place for the *temperature* field and they are *identical for the species (concentration)* field. As Br increases ($Br = 0.5$), the error between the analytical and numerical solutions increases. The difference between the analytical and numerical solutions for the temperature field is more significant for the case of unequal Biot numbers compared to the case for equal Biot numbers. Exact solutions are obtained for the concentration field and hence there is no deviation between analytical and numerical solutions for either case of equal and unequal Biot numbers.

7. CONCLUSIONS

Thermosolutal dissipative chemically reacting flow in a vertical geothermal duct channel containing a non-Darcy porous medium with Robin boundary conditions has been studied theoretically.

The transformed, non-dimensional equations for momentum, energy and species conservation have been solved both with a perturbation method (for low Brinkman number in the absence of Forchheimer drag) and with Runge-Kutta quadrature and a shooting method in the presence of inertial effects. Good correlation of both solutions has been demonstrated in the absence of inertial effects. The simulations have shown that for the small values of Brinkman number, the analytical and numerical solutions agree and the error increases as Brinkman number increases. For the non-Darcy case, an increase in Brinkman number and thermal Grashof number induces significant flow acceleration. With increasing solutal (concentration) Grashof number the velocity distribution is less significantly affected and the flow decreases at the cold wall and increases at the hot wall for both equal and unequal Biot numbers. An increase in homogenous first order chemical reaction parameter decreases the velocity magnitudes. Increasing porous medium (Darcy inverse permeability) parameter and Forchheimer second order inertial parameter both inhibit flow and manifest in strong retardation. The skin friction at the left wall is elevated with greater viscous dissipation (i.e. Brinkman number), chemical reaction parameter whereas it is reduced with increasing thermal Grashof number, concentration Grashof number, porous medium and Forchheimer inertial parameters for both equal and unequal Biot numbers. At the right wall, the skin friction is enhanced with greater thermal Grashof number, concentration Grashof number, Brinkman number and the contrary effect is induced with higher values of chemical reaction parameter, porous medium and Forchheimer inertial parameter. The Nusselt number at the left wall is boosted with greater thermal Grashof number, Brinkman number, chemical reaction parameter whereas it is suppressed with greater concentration Grashof number, porous medium and Forchheimer inertial parameter for equal Biot numbers. At the hot wall the rate of heat transfer (Nusselt number) decreases with an increase in the values of thermal Grashof number, (solutal) concentration Grashof number and Brinkman number and the opposite behavior is generated with an increase in the chemical reaction parameter, porous medium and Forchheimer inertial parameters. Overall the inclusion of viscous dissipation, chemical reaction and Robin (mixed) boundary conditions modifies the transport phenomena characteristics significantly and provides for more realistic simulations of geological (geothermic) double-diffusive convection flows. The current study has been confined to Newtonian fluids. Future studies will consider non-Newtonian models and more complex porous media models of relevance to geothermal energy systems and will be reported soon.

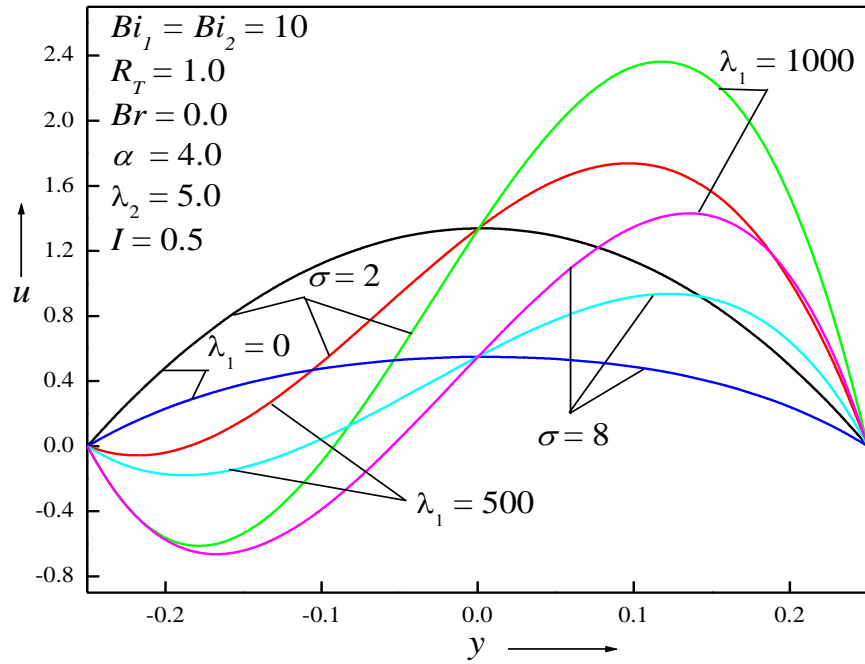


Figure 2 Plots of u for different values of λ_1

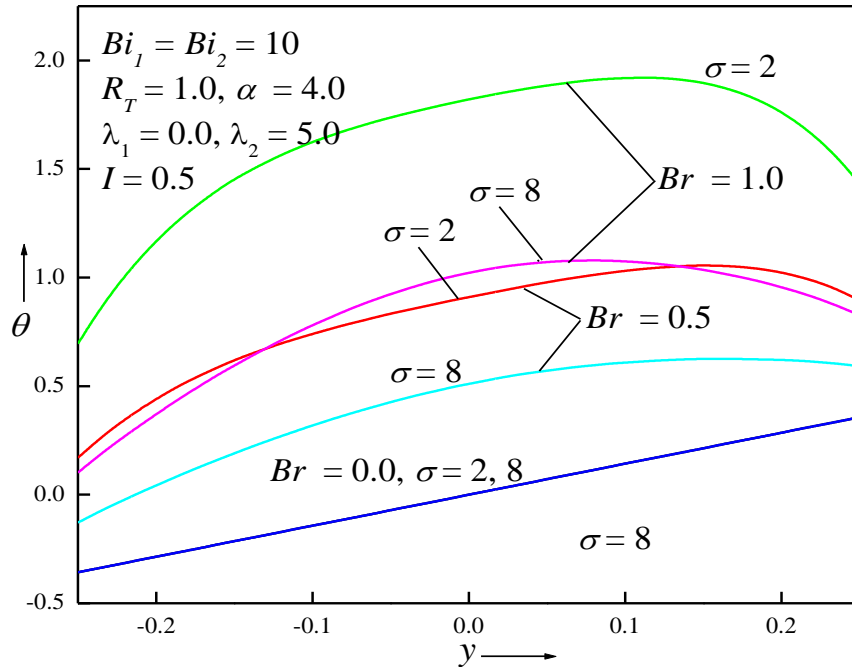


Figure 3 Plots of θ for different values of Br

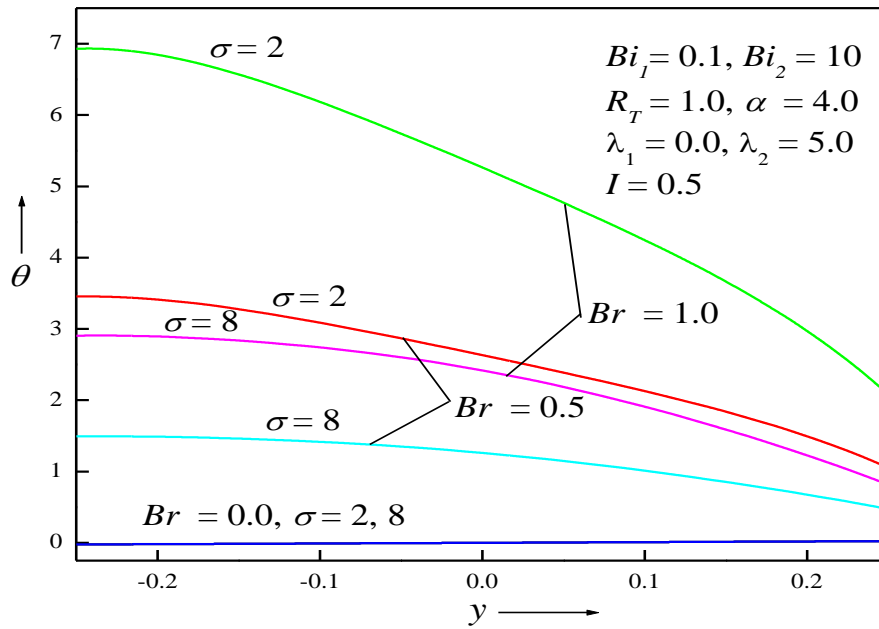


Figure 4 Plots of θ for different values of Br

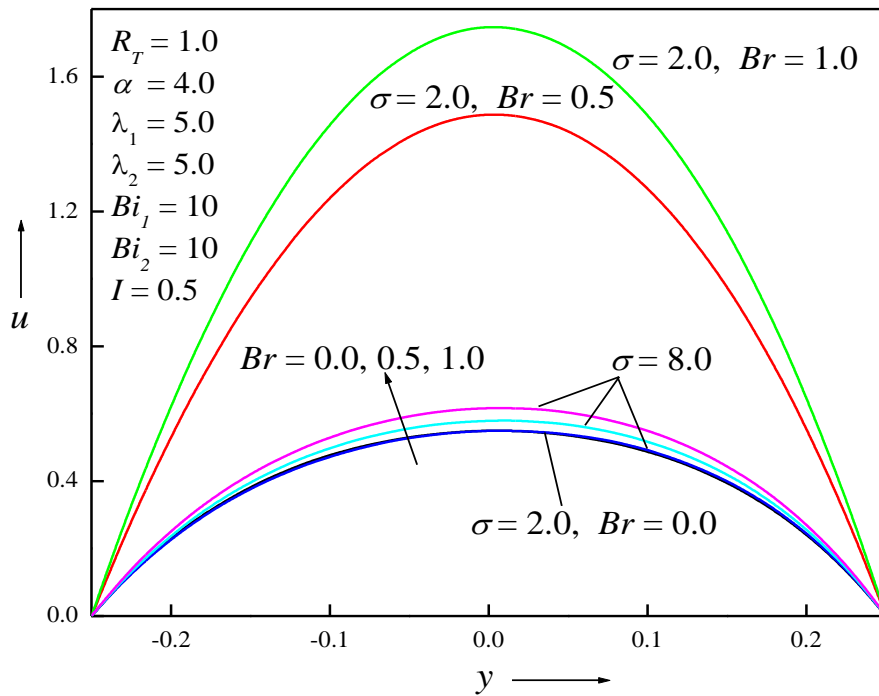
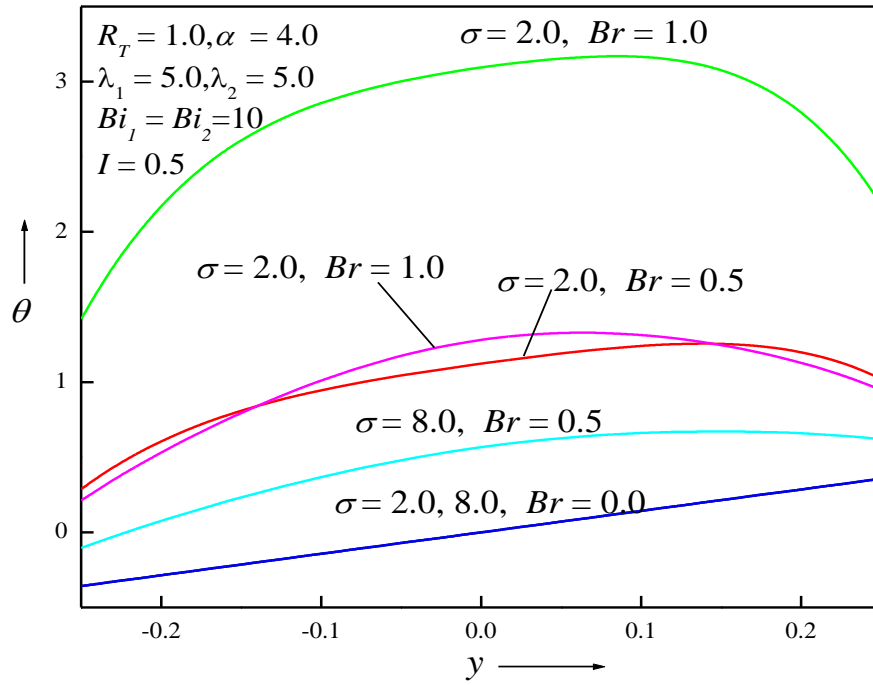
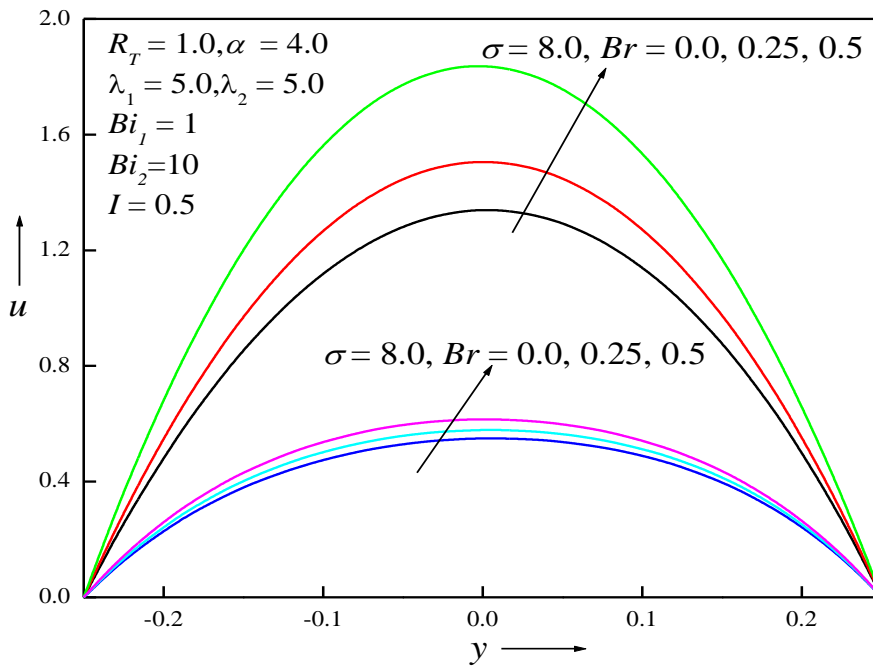


Figure 5 Plots of u for different values of Br

Figure 6 Plots of θ for different values of Br Figure 7 Plots of u for different values of Br

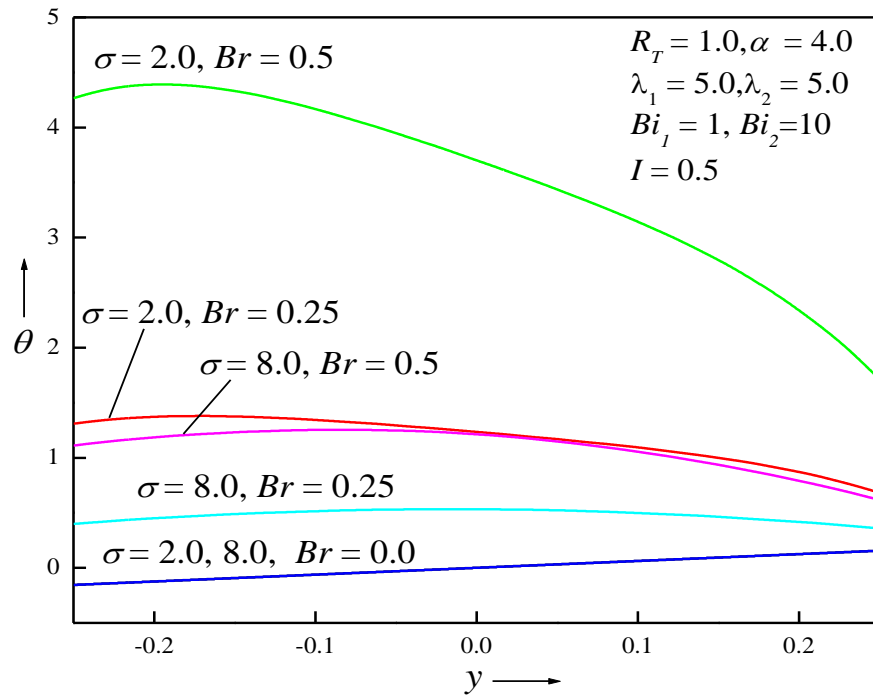


Figure 8 Plots of θ for different values of Br

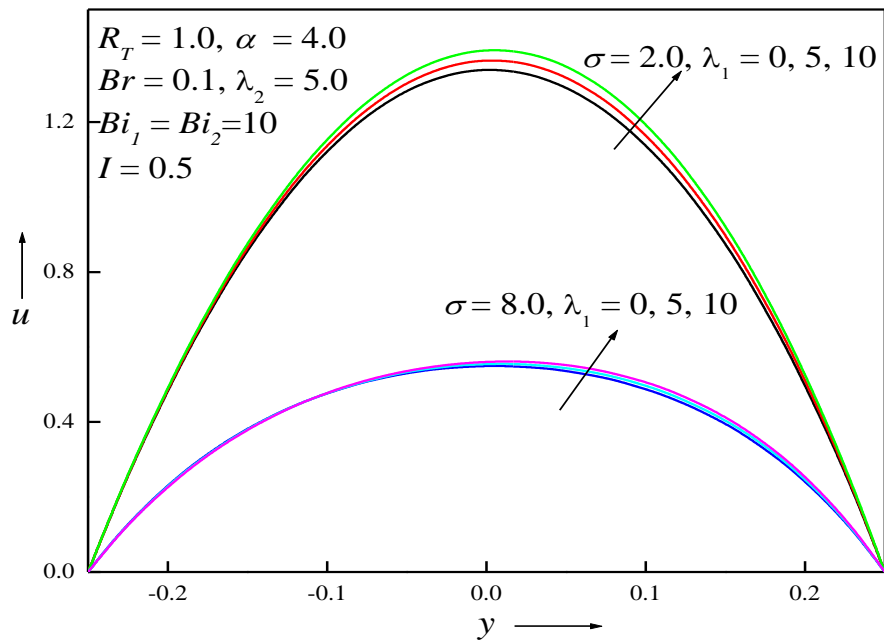


Figure 9 Plots of u for different values of λ_1

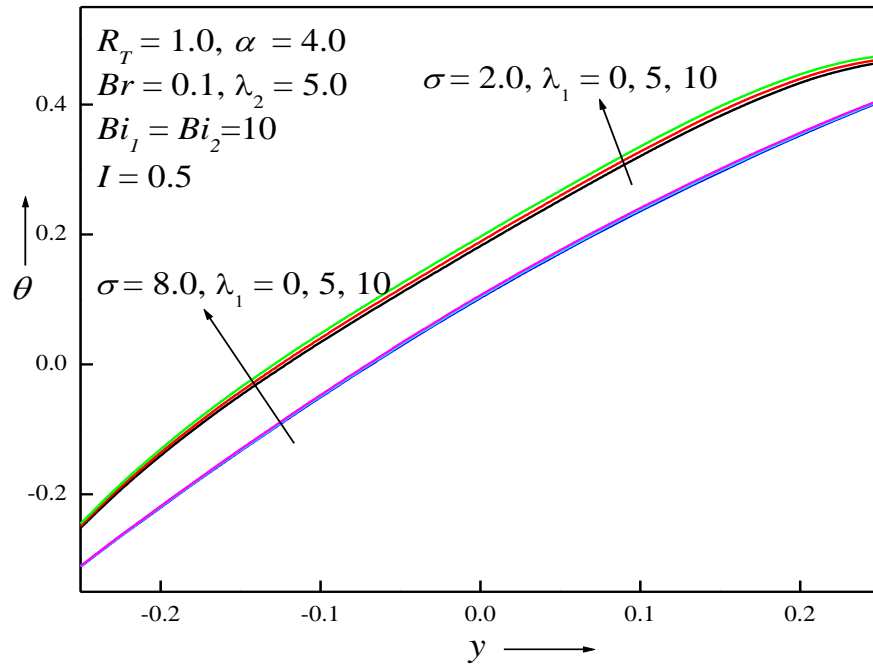


Figure 10 Plots of θ for different values of λ_1

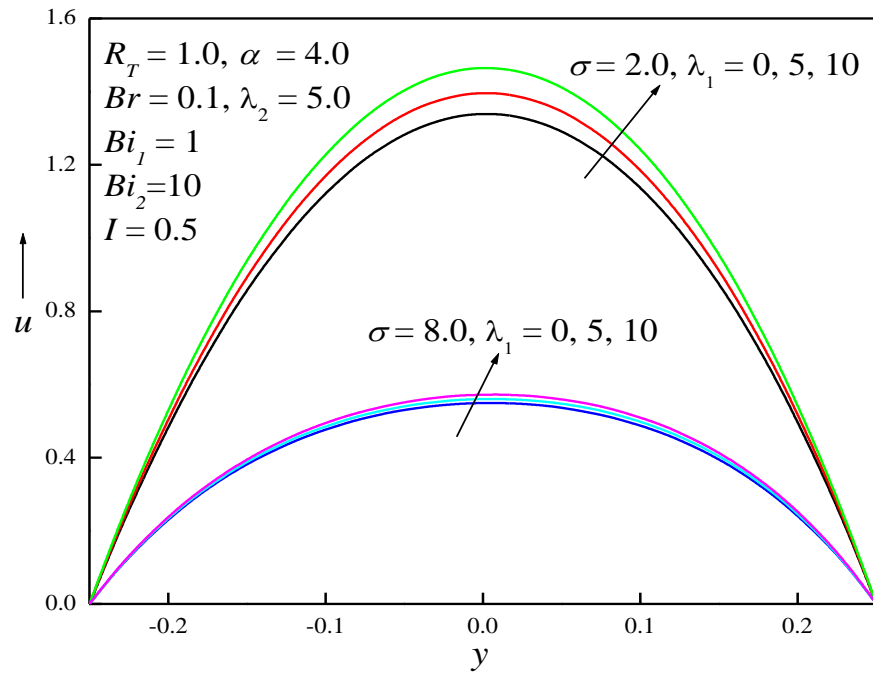


Figure 11 Plots of u for different values of λ_1

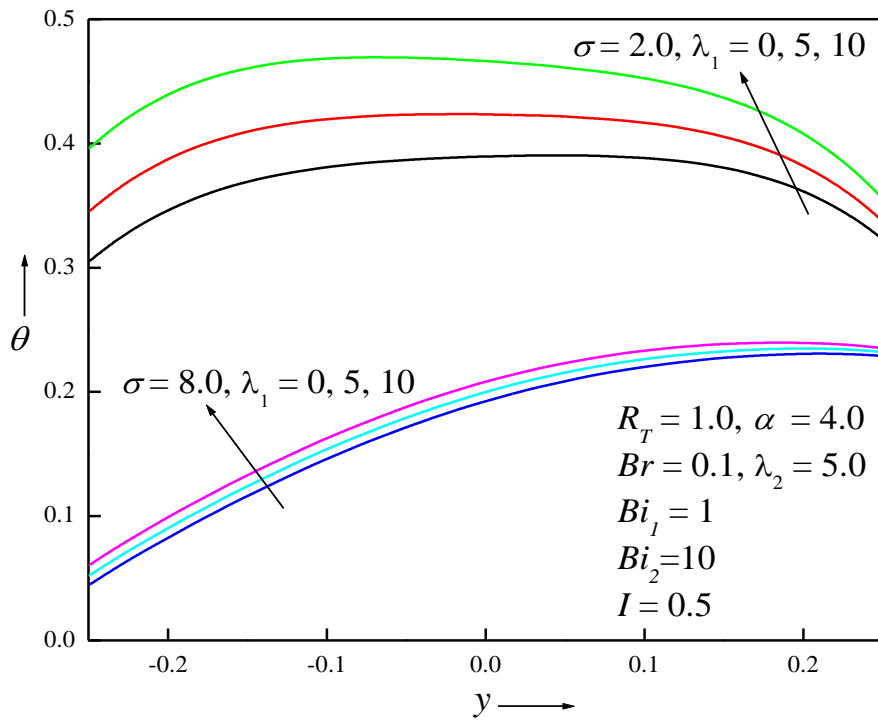


Figure 12 Plots of θ for different values of λ_1

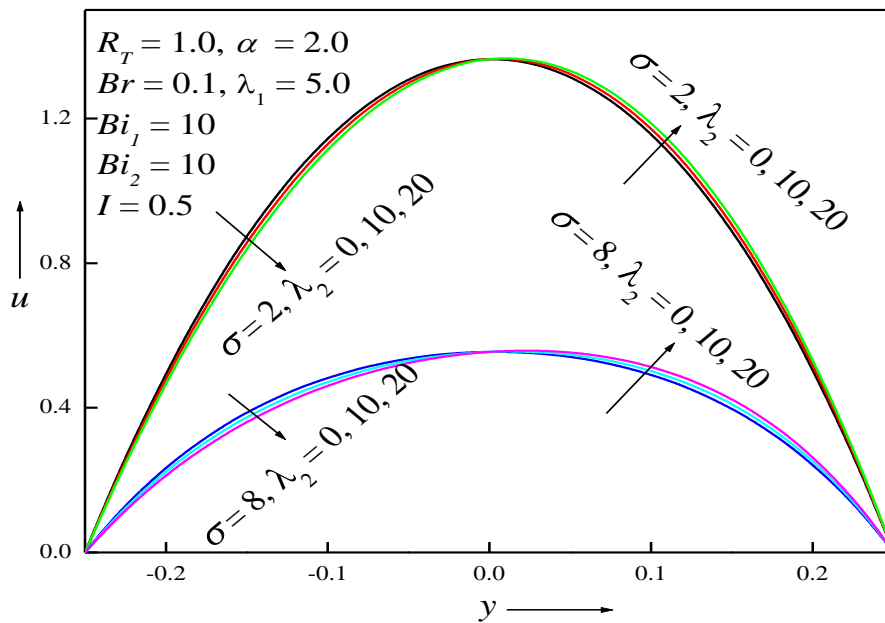


Figure 13 Plots of u for different values of λ_2

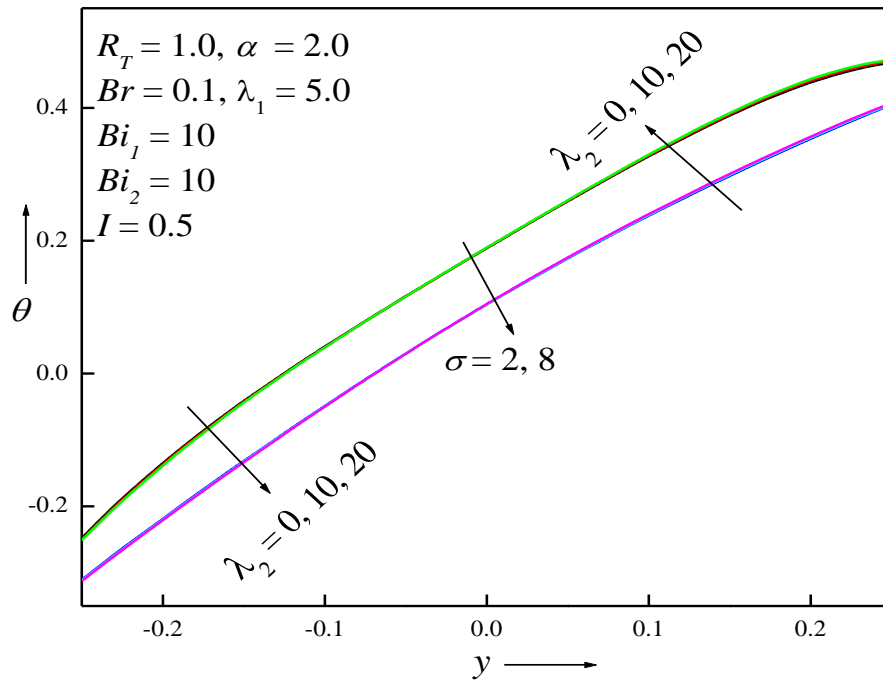


Figure 14 Plots of θ for different values of λ_2

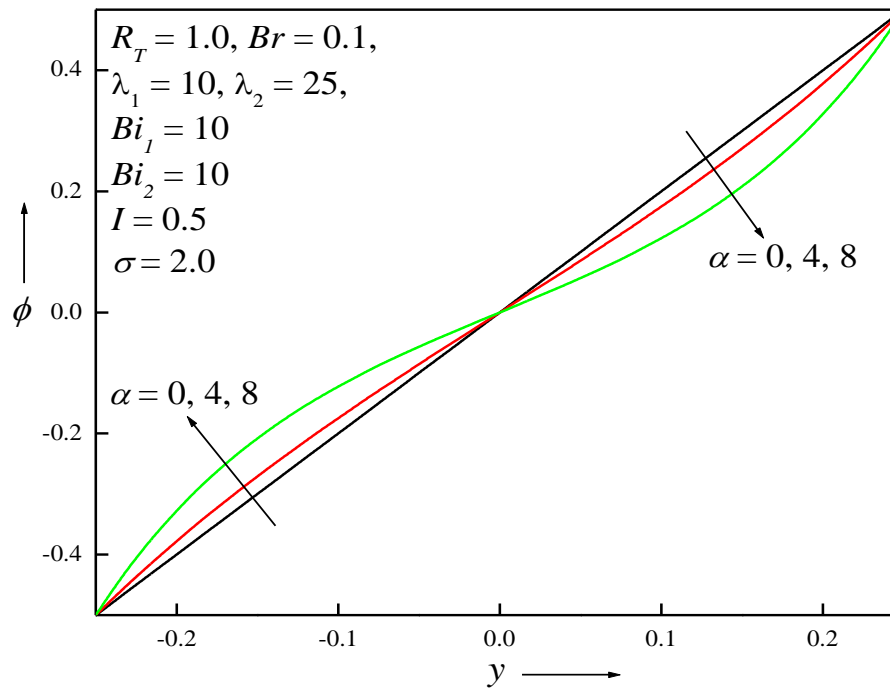


Figure 15 Plots of ϕ for different values of α

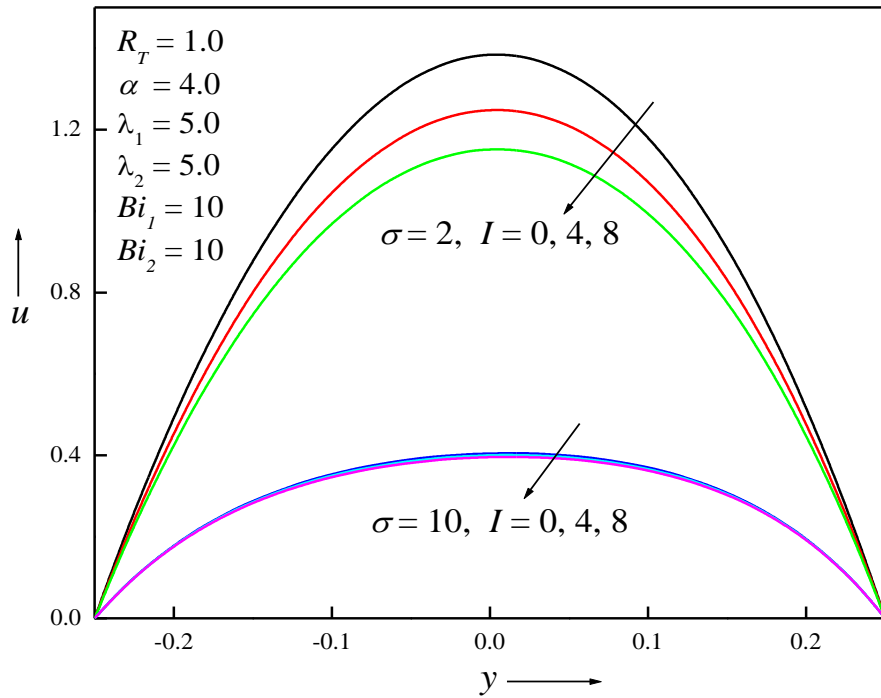


Figure 16 Plots of u for different values of I and σ

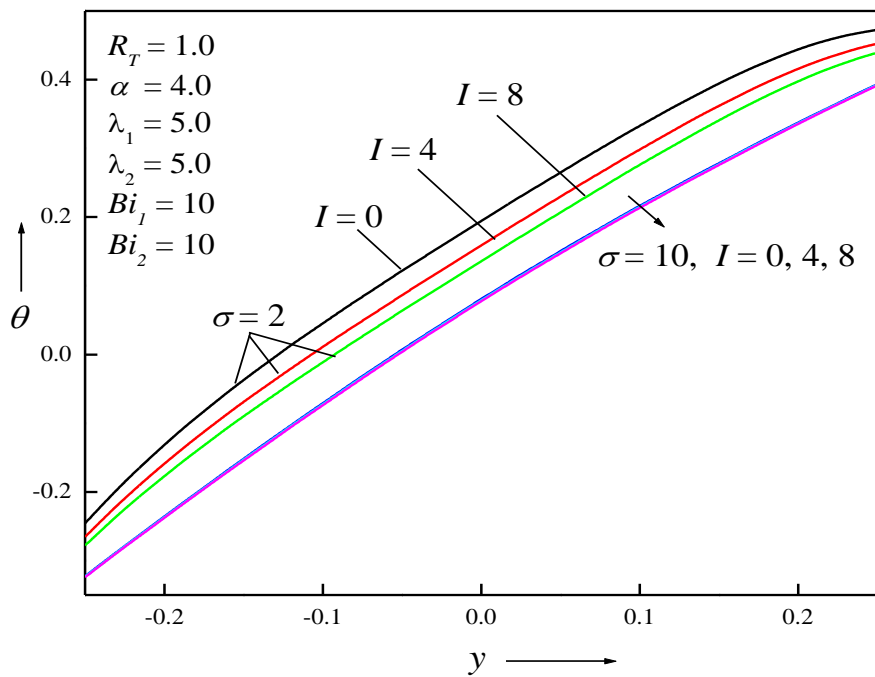
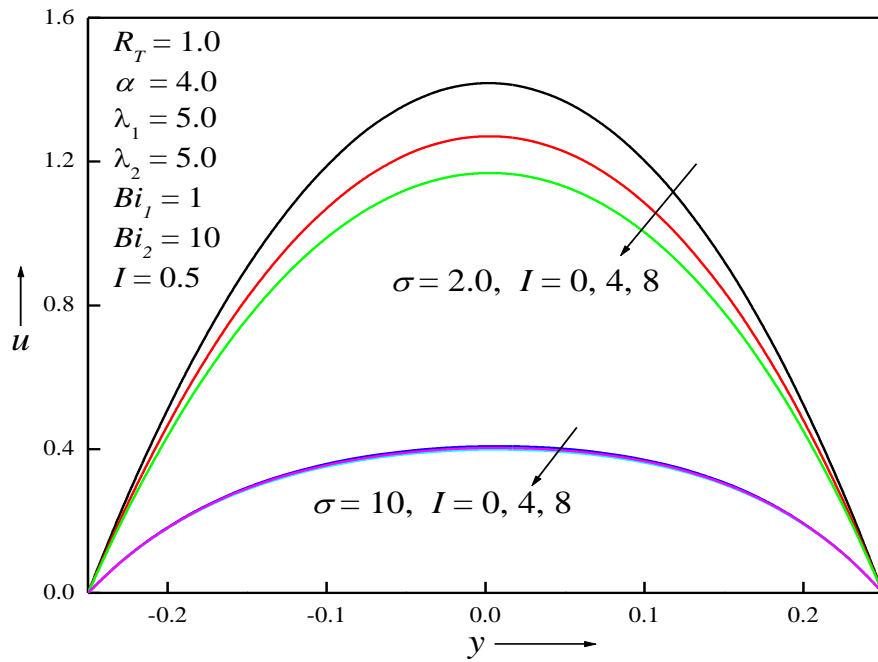
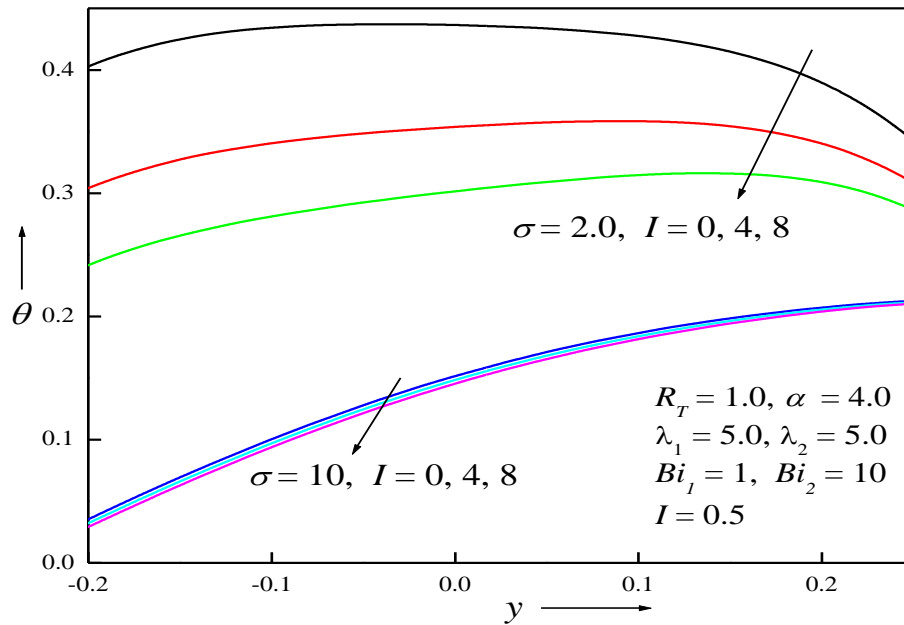


Figure 17 Plots of θ for different values of I and σ

Figure 18 Plots of u for different values of I Figure 19 Plots of θ for different values of I

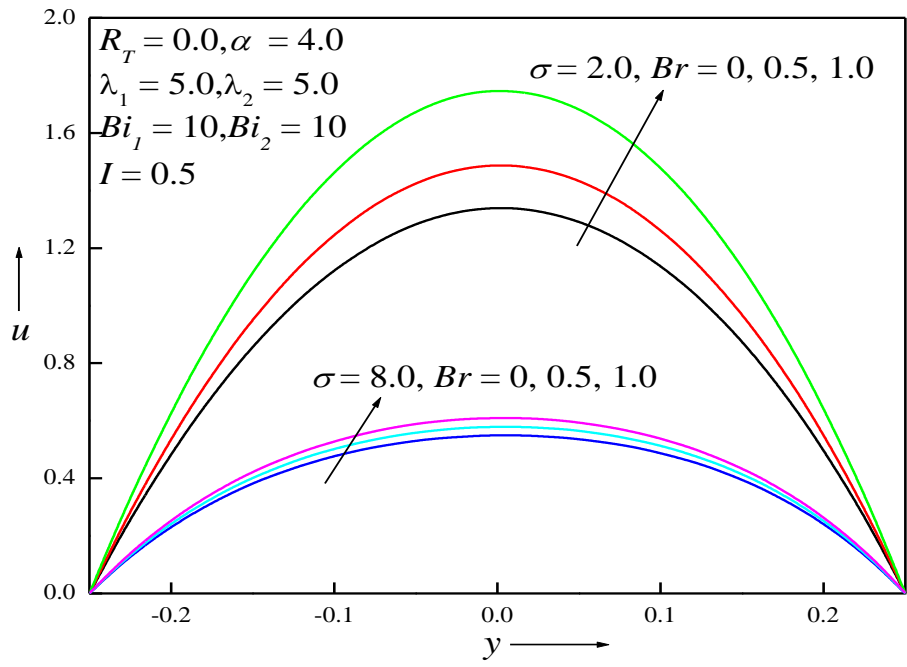


Figure 20 Plots of u for different values of Br

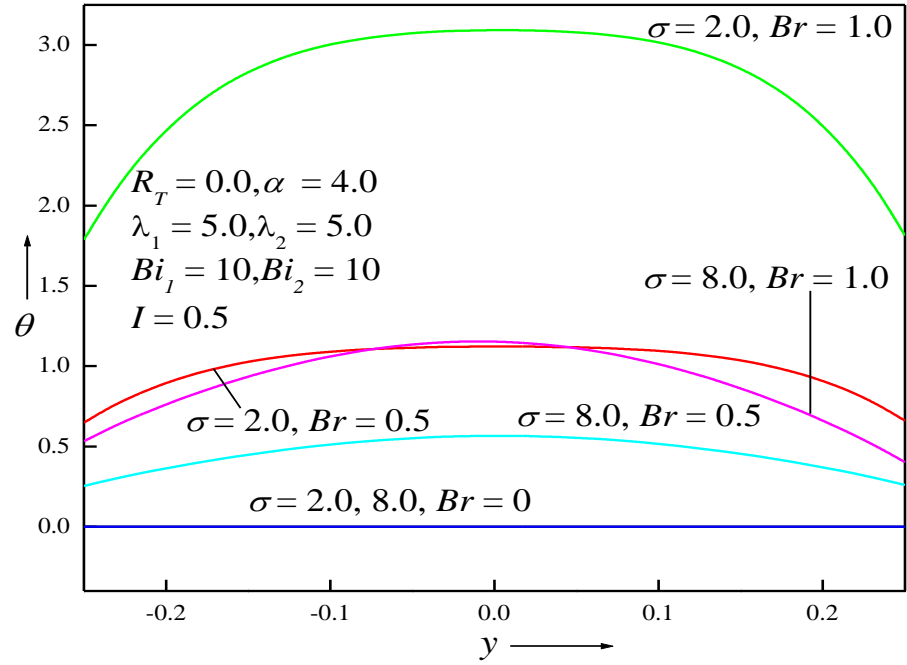


Figure 21 Plots of θ for different values of Br

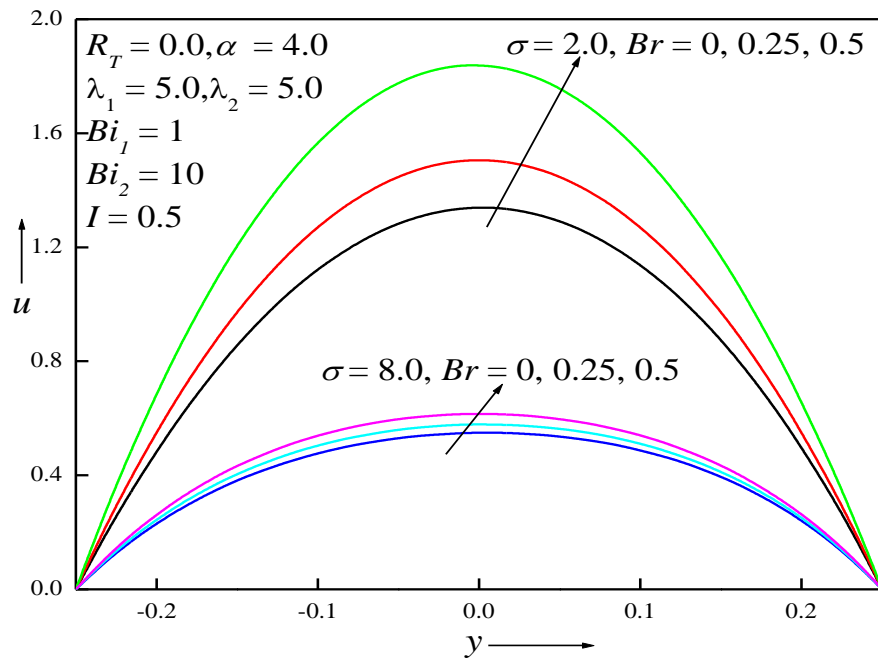
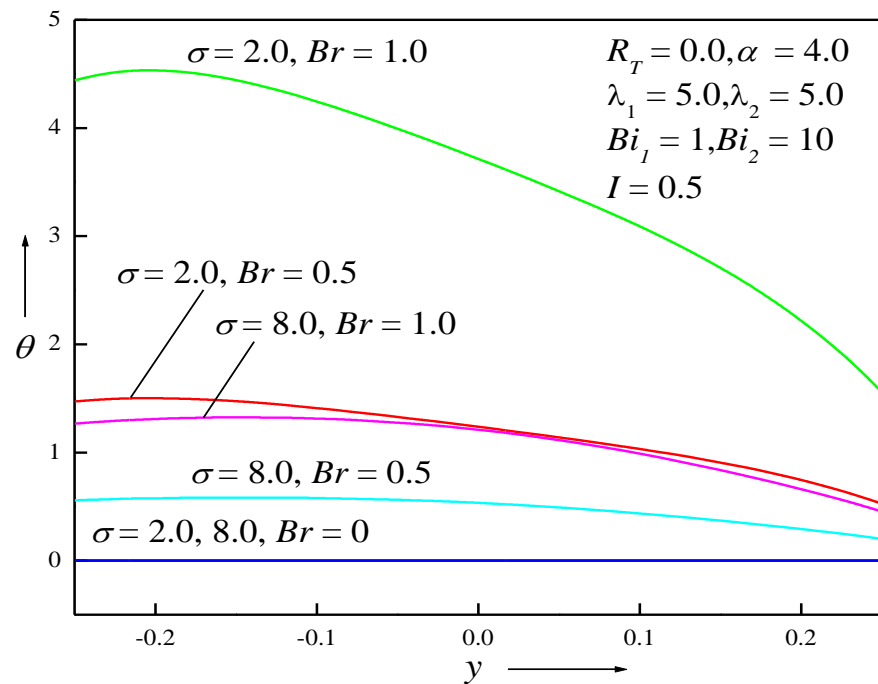
Figure 22 Plots of u for different values of Br Figure 23 Plots of θ for different values of Br

Table 1. Values of skin friction for $R_T=1.0$, $Br = 0.1$, $\lambda_1 = 5.0$, $\lambda_2 = 5.0$, $\alpha = 4.0$, $\sigma=4$, $I=2.0$

	$Bi_1 = 10, Bi_2 = 10$		$Bi_1 = 1, Bi_2 = 10$	
	τ_1	τ_2	τ_1	τ_2
λ_1				
0	8.20961740	-9.66979819	8.20961741	-9.66979817
1	8.02258775	-9.90405984	8.07487173	-9.90808428
10	8.17853069	-10.20209829	8.76825020	-10.28391936
15	8.17471594	-10.48219512	9.12954560	-10.64964620
λ_2				
0	8.92198237	-9.19971245	9.20543493	-9.23294741
10	8.55619963	-9.56564540	8.83568246	-9.59665599
15	8.37333986	-9.74864341	8.65096071	-9.77860981
20	8.19050118	-9.93166244	8.46634234	-9.96062885
Br				
0	8.61880003	-9.26093744	8.69674926	-9.18302219
0.1	8.73908047	-9.38266842	9.02050713	-9.41476862
0.25	8.93370857	-9.57956463	9.60097625	-9.82858396
0.5	9.30448798	-9.95440573	11.00456636	-10.82170361
α				
2	8.73066964	-9.39108481	9.01196010	-9.42310853
4	8.73908047	-9.38266842	9.02050713	-9.41476862
6	8.75094236	-9.37079924	9.03255979	-9.40300648
8	8.76422503	-9.35750902	9.04605371	-9.38983481
σ				
2	10.51822810	-11.18994069	10.89017888	-11.27808897
4	8.73908047	-9.38266842	9.02050713	-9.41476862
6	6.93569686	-7.53849292	7.13590776	-7.52731639
8	5.52045106	-6.07667328	5.66585566	-6.04313955
I				
0	8.95016417	-9.59937974	9.25515002	-9.64623862
4	8.55273965	-9.19117075	8.81516225	-9.21177612
8	8.23576153	-8.86498898	8.46924677	-8.86890439
12	7.97319433	-8.59435797	8.18553630	-8.58680505

Table 2. Values of Nusselt number for $R_T=1.0$, $Br = 0.1$, $\lambda_1 = 5.0$, $\lambda_2 = 5.0$, $\alpha = 4.0$, $\sigma=4$, $I=2.0$

	$Bi_1 = 10, Bi_2 = 10$		$Bi_1 = 1, Bi_2 = 10$	
	Nu_1	Nu_2	Nu_1	Nu_2
λ_1				
0	2.20590246	0.58641333	0.96508232	-0.65440681
1	2.20274019	0.57056862	0.96624557	-0.67561102
10	2.24398751	0.51993840	1.01314568	-0.83307637

15	2.26612337	0.48278372	1.04479064	-0.94909266
λ_2				
0	2.25330114	0.59097032	1.00103041	-0.71926289
10	2.23799593	0.57332905	0.99374506	-0.72683200
15	2.23083496	0.56401640	0.99032844	-0.73141408
20	2.22400171	0.55437568	0.98706252	-0.73652758
Br				
0	1.42857143	1.42857143	0.62500000	0.62500000
0.1	2.24548465	0.58231369	0.99731231	-0.72278159
0.25	3.56829007	-0.78642688	1.66717021	-3.12403029
0.5	6.09162205	-3.39234347	3.29821141	-8.86814262
α				
2	2.24495965	0.58170685	0.99706236	-0.72304286
4	2.24548465	0.58231369	0.99731231	-0.72278159
6	2.24622029	0.58315811	0.99766245	-0.72242132
8	2.24703481	0.58408524	0.99805013	-0.72203008
σ				
2	2.43406463	0.38852539	1.08684360	-1.04457598
4	2.24548465	0.58231369	0.99731231	-0.72278159
6	2.04557087	0.78782259	0.90382367	-0.38627518
8	1.88601903	0.95207874	0.83031980	-0.12121522
I				
0	2.30008798	0.52648241	1.02363517	-0.81726044
4	2.19887822	0.62999707	0.97505296	-0.64284628
8	2.12303228	0.70765867	0.93919988	-0.51400837
12	2.06347537	0.76870215	0.91133820	-0.41380703

Table 3. Values of velocity, temperature and concentration for equal Biot numbers $Bi_1 = Bi_2 = 10$, $R_T = 1.0$, $\lambda_1 = 5.0$, $\lambda_2 = 5.0$, $\alpha = 4.0$, $\sigma = 6.0$, $I = 0.0$

Velocity						
	$Br = 0.0$		$Br = 0.01$		$Br = 0.5$	
y	RPM	RKM	RPM	RKM	RPM	RKM
-0.25	0.0	0.0	0.0	0.0	0.0	0.0
-0.15	0.507763	0.507763	0.508537	0.508388	0.546435	0.543576
-0.05	0.734476	0.734476	0.73566	0.735413	0.793645	0.788179
0.05	0.747206	0.747205	0.74843	0.748146	0.808406	0.801080
0.15	0.534372	0.534371	0.535217	0.535002	0.576642	0.570525
0.25	0.0	0.0	0.0	0.0	0.0	0.0
Temperature						
	$Br = 0.0$		$Br = 0.01$		$Br = 0.5$	
y	RPM	RKM	RPM	RKM	RPM	RKM
-0.25	-0.357152	-0.357142	-0.348766	-0.350897	0.062149	0.000378
-0.15	-0.214291	-0.214285	-0.201573	-0.203530	0.421609	0.401931
-0.05	-0.071430	-0.071428	-0.055591	-0.054356	0.720533	0.668960
0.05	0.071430	0.071428	0.088575	0.084436	0.928667	0.816485

0.15	0.214291	0.214285	0.230340	0.225279	1.016730	0.843386
0.25	0.357152	0.357142	0.368392	0.363628	0.919112	0.727605
	Concentration					
	<i>Br</i> =0.0		<i>Br</i> =0.01		<i>Br</i> =0.5	
<i>y</i>	RPM	RKM	RPM	RKM	RPM	RKM
-0.25	-0.5	-0.5	-0.5	-0.5	-0.5	-0.5
-0.15	-0.270870	-0.270870	-0.270870	-0.270870	-0.270870	-0.270870
-0.05	-0.085660	-0.085660	-0.085660	-0.085660	-0.085660	-0.085660
0.05	0.085660	0.085660	0.085660	0.085660	0.085660	0.085660
0.15	0.270870	0.270870	0.270870	0.270870	0.270870	0.270870
0.25	0.5	0.5	0.5	0.5	0.5	0.5

Table 4. Values of velocity, temperature and concentration for unequal Biot numbers $Bi_1 = 1$, $Bi_2 = 10$, $R_T = 1.0$, $\lambda_1 = 5.0$, $\lambda_2 = 5.0$, $\alpha = 4.0$, $\sigma = 6.0$, $I = 0.0$

	Velocity					
	<i>Br</i> =0.0		<i>Br</i> =0.01		<i>Br</i> =0.5	
<i>y</i>	RPM	RKM	RPM	RKM	RPM	RKM
-0.25	0.0	0.0	0.0	0.0	0.0	0.0
-0.15	0.511053	0.511053	0.512743	0.512223	0.595549	0.592291
-0.05	0.736066	0.736066	0.738781	0.737917	0.871818	0.864793
0.05	0.745616	0.745615	0.748608	0.747613	0.895212	0.884697
0.15	0.531082	0.531081	0.533337	0.532554	0.643856	0.633721
0.25	0.0	0.0	0.0	0.0	0.0	0.0
	Temperature					
	<i>Br</i> =0.0		<i>Br</i> =0.01		<i>Br</i> =0.5	
<i>y</i>	RPM	RKM	RPM	RKM	RPM	RKM
-0.25	-0.156250	-0.156250	-0.141546	-0.146320	0.578967	0.528364
-0.15	-0.093750	-0.093750	-0.068566	-0.075659	1.165420	1.158835
-0.05	-0.031250	-0.031250	0.002975	-0.007365	1.680040	1.628224
0.05	0.031250	0.031250	0.072650	0.058840	2.101260	1.952966
0.15	0.093750	0.093750	0.140007	0.122945	2.406610	2.131153
0.25	0.156250	0.156250	0.203940	0.184566	2.540730	2.134406
	Concentration					
	<i>Br</i> =0.0		<i>Br</i> =0.01		<i>Br</i> =0.5	
<i>y</i>	RPM	RKM	RPM	RKM	RPM	RKM
-0.25	-0.5	-0.5	-0.5	-0.5	-0.5	-0.5
-0.15	-0.270870	-0.270870	-0.270870	-0.270870	-0.270870	-0.270870
-0.05	-0.085660	-0.085660	-0.085660	-0.085660	-0.085660	-0.085660
0.05	0.085660	0.085660	0.085660	0.085660	0.085660	0.085660
0.15	0.270870	0.270870	0.270870	0.270870	0.270870	0.270870
0.25	0.5	0.5	0.5	0.5	0.5	0.5

REFERENCES

- [1] M. Kaviany, *Principles of Heat Transfer in Porous Media*, Second Ed. Springer, New York, (1995).
- [2] D.A. Nield, A. and Bejan, *Convection in Porous Media*, Fourth Ed., Springer, New York, (2013).
- [3] D.B. Ingham, I. Pop, *Transport Phenomena in Porous Media*, Second Edn. Pergamon, Oxford, (2002).
- [4] O.M. Phillips, *Geological Fluid Dynamics: sub-surface flow and reactions*. Cambridge University Press, UK (2009).
- [5] D. Gupta, L. Kumar, O. Anwar Bég, B. Singh, Finite element analysis of transient heat and mass transfer in microstructural boundary layer flow from porous stretching sheet, *Comp. Thermal Sci.* 6 (2014), 155-169.
- [6] M. Mamou, P. Vasseur, E. Bilgen, Multiple solutions for double-diffusive convection in a vertical porous enclosure, *Int. J. Heat Mass Transfer*, 38, (1995) 1787–1798.
- [7] P. A. Lakshmi Narayana and P.V. Murthy, Soret and Dufour effects on free convection heat and mass transfer from a horizontal flat plate in a Darcy porous medium, *ASME J. Heat Transfer* 130 (2008) 104504
- [8] V. Prasad and F.A. Kulacki, Natural convection in porous media bounded by short concentric vertical cylinders, *ASME J. Heat Transf.*, 107 (1985) 147–154.
- [9] P. Vasseur, C.H. Wang and M. Sen, Natural convection in an inclined rectangular porous slot: Brinkman extended Darcy model, *ASME J. Heat Transf.*, 112 (1990) 507–511.
- [10] J.C. Umavathi, J.P. Kumar, A.J. Chamkha, and I. Pop, Mixed convection in a vertical porous channel, *Transp. Porous Media*, 61 (2005) 315–335.
- [11] J.C. Umavathi, Mallikarjun, B., Patil and Pop, I., On laminar mixed convection flow in a vertical porous stratum with symmetric wall heating conditions, *Int. J. Trans. Phenomenon*, 8 (2006) 127–140.
- [12] J.C. Umavathi, J. Prathap Kumar and J. Sultana, Mixed convection flow in a vertical porous channel with boundary conditions of third kind with heat source/sink, *J. Porous Media*, 15 (2012) 998–1007.
- [13] J.C. Umavathi, A.S.V. Ravi Kanth and M. Shekar, Mixed convective flow in a vertical channel filled with porous medium using Differential Transform Method, *Int. J. Math. Arch.*, 4 (2013) 1–9.
- [14] H.C. Brinkman, On the permeability of media consisting of closely packed porous particles, *Appl. Sci. Res. A*, 1 (1947) 81–86.
- [20] P. Forchheimer, Wasserbewegung durch Boden. *Z. Ver. Deut. Ing.*, 45 (1901) 1736–1741.
- [21] O. Anwar Bég, J. Zueco and H.S. Takhar, Laminar free convection from a continuously moving vertical surface in a thermally stratified, non-Darcian high-porosity medium: Network numerical study, *Int. Comm. Heat Mass Transfer*, 35 (2008), 7, 810-816.
- [22] C-Y. Cheng, Non-Darcy natural convection heat and mass transfer from a vertical wavy surface in saturated porous media, *Applied Mathematics and Computation*, 182 (2006) 1488-1500.
- [23] S.K. Jena *et al.*, Thermosolutal convection in a fluid-porous composite medium, *Heat Transfer-Asian Research*, 42 (2013)_281-299.
- [24] T. A. Bég, M.M. Rashidi, O. Anwar Bég and N. Rahimzadeh, DTM semi-numerical simulation of biofluid-particle suspension flow and heat transfer in non-Darcian porous media, *Computer Methods Biomechanics Biomedical Engineering*, 16 (2013) 896-907.
- [25] Z. Chen *et al.*, Derivation of the Forchheimer law via homogenization, *Transp. Porous Media*, 44 (2001) 325-335.
- [26] Whitaker, S. The Forchheimer equation: A theoretical development, *Transport in Porous Media* 25 (1996), 27–61.

- [27] M. Sener *et al.*, Forchheimer forced convection in a rectangular channel partially filled with aluminum foam, *Experimental Thermal and Fluid Science*, 75 (2016) 162-172.
- [28] J. Ennis-King and L Paterson, Coupling of geochemical reactions and convective mixing in the long-term geological storage of carbon dioxide, *International Journal of Greenhouse Gas Control*, 1 (2007) 86-93.
- [29] Islam, A. W., Lashgari, H. R. & Sephernoori, K. Double diffusive natural convection of CO₂ in a brine saturated geothermal reservoir: Study of non-modal growth of perturbations and heterogeneity effects. *Geotherm.* 51 (2014) 325–336.
- [30] Ward, T., Jensen, O., Power, H. & Riley, D. High-Rayleigh-number convection of a reactive solute in a porous medium. *J. Fluid Mech.* 760 (2014), 95–126.
- [31] X-F. Li *et al*, Simulation of gas exothermic chemical reaction in porous media reactor with lattice Boltzmann method, *J. Thermal Science*, 22 (2013) 42–47.
- [32] Shamshuddin MD, Siva Reddy Sheri and O Anwar Bég, Oscillatory dissipative conjugate heat and mass transfer in chemically reacting micropolar flow with wall couple stress: A finite element numerical study, *Proc IMechE Part E: J Process Mechanical Engineering* 233 (2019) 48–64.
- [33] M.M. Rashidi, M. Ferdows, Md. Jashim Uddin, O. Anwar Bég and N. Rahimzadeh, Group theory and differential transform analysis of mixed convective heat and mass transfer from a horizontal surface with chemical reaction effects, *Chemical Engineering Communications*, 199 (2012) 1012-1043.
- [34] S.P. Anjali Devi, R. Kandasamy, Effects of chemical reaction, heat and mass transfer on laminar flow along a semi-infinite horizontal plate, *Heat Mass Transfer*, 35 (1999) 465-467.
- [35] A. Postelnicu, Influence of chemical reaction on heat and mass transfer by natural convection from vertical surfaces in porous media considering Soret and Dufour effects, *Heat Mass Transfer*, 43 (2007) 595-602.
- [36] A.M. Rashad, and S.M.M. EL-Kabeir, Heat and mass transfer in transient flow by mixed convection boundary layer over a stretching sheet embedded in a porous medium with chemically reactive species, *J. Porous Media*, 13 (2010) 75-85.
- [37] R. Kandasamy, I. Muhaimin and R. Hashim, Thermophoresis and chemical reaction effects on non-Darcy mixed convective heat and mass transfer past a porous wedge with variable viscosity in the presence of suction or injection, *Nuclear Engineering and Design*, 238 (2008) 2699-2705.
- [38] J. Zueco, O. Anwar Bég, Tasveer A. Bég and H.S. Takhar, Numerical study of chemically reactive buoyancy-driven heat and mass transfer across a horizontal cylinder in a high-porosity non-Darcian regime, *J. Porous Media*, 12 (2009) 519-535.
- [39] H.D. Nguyen *et al.*, Unsteady non-Darcy reaction-driven flow from an anisotropic cylinder in porous media, *Chem Eng. Sci*, 51 (1996) 4963-4977.
- [40] E. Zanchini, Effect of viscous dissipation on mixed convection in a vertical channel with boundary conditions of the third kind, *Int. J. Heat Mass Transfer*, 41 (1998) 3949–3959.
- [41] J.C. Umavathi, J. Prathap Kumar, J. Sultana, Mixed convection flow in a vertical channel with boundary conditions of the third kind in the presence of heat source/sink, *Appl. Math. Mech.*, 33 (2012) 1015–1034.
- [42] J.C. Umavathi and S. Veershetty, Non-Darcy mixed convection in a vertical porous channel with boundary conditions of third kind, *Trans. Porous Media*, 95 (2012) 111-131.
- [43] W. Leng *et al.*, Viscous heating, adiabatic heating and energetic consistency in compressible mantle convection, *Geophysical J. International*, 173 (2014) 693-702.
- [44] M. Norouzi, S. Dorrani, H. Shokri and O. Anwar Bég, CFD simulation of viscous dissipation effects on miscible thermo-viscous fingering instability in porous media, *Int. J. Heat Mass Transfer*, 129 (2019) 212-223.

- [45] J.C. Umavathi and M.A. Sheremet, Mixed convection flow of an electrically conducting fluid in a vertical channel using Robin boundary conditions with heat source or sink, *European J. Mechanics B. Fluids*, 55 (2016) 132-145.
- [46] O. Anwar Bég, M. Faisal Md Basir, M.J. Uddin, and A. I. Md. Ismail, Numerical study of slip effects on asymmetric bioconvective nanofluid flow in a porous microchannel with an expanding/contracting upper wall using Buongiorno's model, *J. Mechanics in Medicine and Biology*, 17 (2017) 1750059.1-1750059.28.
- [47] O. Anwar Bég, Tasveer A. Bég, I. Karim, M. S. Khan, M. M. Alam, M Ferdows, M. Shamshuddin, Numerical study of magneto-convective heat and mass transfer from inclined surface with Soret diffusion and heat generation effects: A model for ocean magnetohydrodynamic energy generator fluid dynamics, *Chinese J. Physics* (2019). doi.org/10.1016/j.cjph.2019.05.002 (14 pages)
- [48] B. Gebhart *et al.* *Buoyancy-induced Flows and Transport*, Hemisphere, Washington, USA (1988).
- [49] Lai, FC and Kulacki, FA, Non-Darcy convection from horizontal impermeable surfaces in saturated porous media, *Int. J. Heat and Mass Transfer*, 30 (1987), 2189-2192.
-